Chapter 2
Low-Frequency Magnetoelectric Effects in Magnetostrictive-Piezoelectric Composites

Abstract In this chapter, we discuss the theoretical modeling of low-frequency ME effect in layered and bulk composites based on magnetostrictive and piezoelectric materials. Our analysis rests on the effective-medium approach and exact calculation based on elastostatic, electrostatic and magnetostatic equations. The expressions for effective parameters including ME susceptibilities and ME voltage coefficients as functions of material parameters and volume fractions of components are obtained. Longitudinal, transverse and in-plane field orientations are considered. The use of the offered model has allowed to estimate the ME effect in ferrite cobalt–barium titanate, ferrite cobalt–PZT, ferrite nickel–PZT, lanthanum-strontium manganite–PZT composites adequately.

2.1 Symmetric Layered Structures

Using layered structures enables one to overcome a series of difficulties that are characteristic for bulk composites. The reasons for the giant ME effects in layered composites are: (a) high piezoelectric and piezomagnetic coefficients in individual layers, (b) effective stress transfer between layers, (c) ease of poling and subsequent achievement of a full piezoelectric effect, and (d) ability to hold charge due to suppression of leakage currents across composites with a 2–2 connectivity.

Prior theoretical models based on mechanics and constitutive relationships by Harshe et al. (1993) were restricted to account for longitudinal ME voltage coefficient in laminates having ideal mechanical connection at the interfaces between layers. Principal disadvantages of this earlier approach were as follows: (i) For the case of longitudinally oriented fields, the effect of the magnetic permeability of the ferrite phase was ignored. Diminution of interior (local) magnetic fields results in a weakening of ME interactions via demagnetization fields. (ii) The case of fields applied in cross orientations to the ME layer connectivity was not considered, which later experimental investigations revealed large ME responses.

M. Bichurin and V. Petrov, *Modeling of Magnetoelectric Effects in Composites*, Springer Series in Materials Science 201, DOI: 10.1007/978-94-017-9156-4_2,

In this work, we present a summary of a more recent theory of ME laminate composites, which are free from the disadvantages mentioned just above. The approach is based on continuum mechanics, and considers the composite as a homogeneous medium having piezoelectric and magnetostrictive subsystems. To derive the effective material parameters of composites, an averaging method consisting of two steps (Bichurin et al. 2002a, b, 2003, 2009; Gheevarughese et al. 2007) should be used. In the first step, the composite is considered as a structure whose magnetostrictive and piezoelectric phases are distinct and separable. ME composites are characterized by the presence of magnetic and electric subsystems interacting with each other.

The constitutive equation for the piezoelectric effect can be given in the following form:

$$ {}^{p}S_i = {}^{p}s_{ij}{}^{p}T_j + {}^{p}d_{ki}{}^{p}E_k, \tag{2.1} $$

$$ {}^{p}D_k = {}^{p}d_{ki}{}^{p}T_i + {}^{p}\varepsilon_{kn}{}^{p}E_n; \tag{2.2} $$

where ${}^{p}S_i$ is a strain tensor component of the piezoelectric phase; ${}^{p}E_k$ is a vector component of the electric field; ${}^{p}D_k$ is a vector component of the electric displacement; ${}^{p}T_i$ is a stress tensor component of the piezoelectric phase; ${}^{p}s_{ij}$ is a compliance coefficient of the piezoelectric phase; ${}^{p}d_{ki}$ is a piezoelectric coefficient of the piezoelectric phase; and ${}^{p}\varepsilon_{kn}$ is a permittivity matrix of the piezoelectric phase.

Analogously, the strain and magnetic induction tensors of the magnetostrictive phase are respectively

$$ {}^{m}S_i = {}^{m}s_{ij}^{m}T_j + {}^{m}q_{ki}{}^{m}H_k, \tag{2.3} $$

$$ {}^{m}B_k = {}^{m}q_{ki}{}^{m}T_i + {}^{m}\mu_{kn}{}^{m}H_n, \tag{2.4} $$

where ${}^{m}S_i$ is a strain tensor component of the magnetostrictive phase; ${}^{m}T_j$ is a stress tensor component of the magnetostrictive phase; ${}^{m}s_{ij}$ is a compliance coefficient of the magnetostrictive phase; ${}^{m}H_k$ is a vector component of magnetic field; ${}^{m}B_k$ is a vector component of magnetic induction; ${}^{m}q_{ki}$ is a piezomagnetic coefficient; and ${}^{m}\mu_{kn}$ is a permeability matrix.

Prior models assumed that the connection at interfaces between layers was ideal. However, in this chapter, we assume that there is a coupling parameter $k = ({}^{p}S_i - {}^{p}S_{i0})/({}^{m}S_i - {}^{p}S_{i0})$ $(i = 1, 2)$, where ${}^{p}S_{i0}$ is a strain tensor component assuming no friction between layers (Bichurin et al. 2003). This interphase–interface elastic–elastic coupling parameter depends on interface quality, and is a measure of a differential deformation between piezoelectric and magnetostrictive layers. The coupling parameter is $k = 1$ for the case of an ideal interface, and *is* $k = 0$ for the case of no friction.

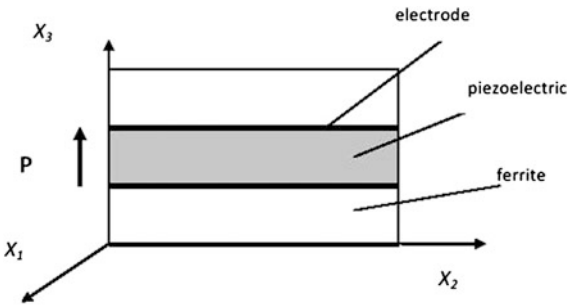

Fig. 2.1 Schematic of the layered composite structure

In the second step of the averaging method to derive the effective materials parameters, the bilayer composite is considered as a homogeneous solid, whose behavior can be described by the following coupled sets of linear algebraic equations:

$$\begin{aligned} S_i &= s_{ij}T_j + d_{ki}E_k + q_{ki}H_k, \\ D_k &= d_{ki}T_i + \varepsilon_{kn}E_n + \alpha_{kn}H_n, \\ B_k &= q_{ki}T_i + \alpha_{kn}E_n + \mu_{kn}H_n; \end{aligned} \tag{2.5}$$

where S_i is a strain tensor component; T_j is a stress tensor component; E_k is a vector component of the electric field; D_k is a vector component of the electric displacement; H_k is a vector component of the magnetic field; B_k is a vector component of the magnetic induction; s_{ij} is an effective compliance coefficient; d_{ki} is a piezoelectric coefficient; q_{ki} is a piezomagnetic coefficient; ε_{kn} is an effective permittivity; μ_{kn} is a permeability coefficient; and α_{kn} is a ME coefficient.

The simultaneous solution of the coupled sets of linear algebraic equations allows one to find the effective parameters of a composite.

Let us consider that the layers of a composite are oriented along the planes (X_1, X_2), and that the direction X_3 is perpendicular to the same plane. In this case, the direction of polarization in a sample coincides with the X_3 axis. If we by choice apply a constant magnetic bias and variable magnetic field along the same direction coincidental with that of the polarization, then any resultant electric field will also be parallel to the X_3 axis, as shown in Fig. 2.1. This summarization supposes that the symmetry of the piezoelectric phase is ∞m, and that of the magnetic phase is cubic. The following boundary conditions can then be used to derive expressions for ME coefficients.

$$\begin{aligned} {}^{p}S_i &= k^{m}S_i + (1-k)^{p}S_{i0}; \quad (i = 1, 2) \\ {}^{p}T_i &= -{}^{m}T_i(1-v)/v; \quad (i = 1, 2) \end{aligned} \tag{2.6}$$

where $v = pv/(pv + {}^{m}v)$, ${}^{p}v$ and ${}^{m}v$ denote the Poisson's ratio of the piezoelectric and magnetostrictive phases, respectively; and pS_{10} and pS_{20} are the strain tensor components for $k = 0$.

Using continuity conditions for magnetic and electric fields, and using open circuit condition, one can then obtain the following expressions for the ME susceptibility, and longitudinal ME voltage coefficient.

$$\begin{aligned}\alpha_{33} &= 2\frac{k\mu_0(v-1)^p d_{31}{}^m q_{31}}{[\mu_0(v-1) - {}^m\mu_{33}v][kv({}^m s_{12}+{}^m s_{11}) - ({}^p s_{11}+{}^p s_{12})(v-1)] + 2{}^m q_{31}^2 kv^2};\\ \alpha_{E,33} &= \frac{E_3}{H_3} = 2\frac{\mu_0 kv(1-v)^p d_{31}{}^m q_{31}}{\{2{}^p d_{31}^2(1-v) + {}^p\varepsilon_{33}[({}^p s_{11}+{}^p s_{12})(v-1) - v({}^m s_{11}+{}^m s_{12})]\}}\\ &\quad\times\frac{[({}^p s_{11}+{}^p s_{12})(v-1) - kv({}^m s_{11}+{}^m s_{12})]}{\{[\mu_0(v-1) - {}^m\mu_{33}v][kv({}^m s_{12}+{}^m s_{11}) - ({}^p s_{11}+{}^p s_{12})(v-1)] + 2{}^m q_{31}^2 kv^2\}}\end{aligned} \tag{2.7}$$

The earlier expression obtained by Harshe et al. (1993) matched to our theory for the special case of $k = 1$, provided that the magnetic field is applied only to the ferrite phase.

The model presented above allows for the determination of the longitudinal ME coefficients as functions of volume fractions, physical parameters of phases, and elastic–elastic interfacial coupling parameter k.

Next we consider the transverse fields' orientation that corresponds to E and δE being applied along the X_3 direction, and H and δH along the X_1 direction (in the sample plane). The expressions for the ME susceptibility, and transverse ME voltage coefficient are then respectively

$$\begin{aligned}\alpha_{31} &= \frac{(v-1)\mathrm{v}({}^m q_{11}+{}^m q_{21})^p d_{31} k}{(v-1)({}^p s_{11}+{}^p s_{12}) - kv({}^m s_{11}+{}^m s_{12})},\\ \alpha_{E,31} &= \frac{E_3}{H_1} = \frac{-kv(1-v)({}^m q_{11}+{}^m q_{21})^p d_{31}}{{}^p\varepsilon_{33}({}^m s_{12}+{}^m s_{11})kv + {}^p\varepsilon_{33}({}^p s_{11}+{}^p s_{12})(1-v) - 2k^p d_{31}^2(1-v)}.\end{aligned} \tag{2.8}$$

Finally, we consider a bilayer laminate that is poled with an electric field E in the plane of the sample. We suppose that the in-plane fields H and δH are parallel, and that the induced electric field δE is measured in the same direction (i.e., along the c-axis). Expression for the α, can be obtained in the following form.

$$\begin{aligned}\alpha_{E,11} = &\{[{}^m q_{11}({}^p s_{33}{}^p d_{11} - {}^p s_{12}{}^p d_{12}) + {}^m q_{12}({}^p s_{11}{}^p d_{12} - {}^p s_{12}{}^p d_{11})](1-v)\\ &+[{}^m q_{11}({}^m s_{11}{}^p d_{11} - {}^m s_{12}{}^p d_{12}) + {}^m q_{12}({}^m s_{11}{}^p d_{12} - {}^m s_{12}{}^p d_{11})]vk\}vk(1-v)/\\ &\{[(1-p){}^m\varepsilon_{11} + v^p\varepsilon_{11}][(1-v)^2({}^p s_{11}{}^p s_{33} - {}^p s_{12}^2)\\ &+(1-v)vk({}^m s_{11}{}^p s_{11} + {}^p s_{33}{}^m s_{11} - 2{}^p s_{12}{}^m s_{12})]\\ &+k^2v^2({}^m s_{11}^2 - {}^m s_{12}^2) - kv(1-v)^2(2{}^p s_{12}{}^p d_{11}{}^p d_{12} - {}^p s_{33}{}^p d_{11}^2\\ &- {}^p s_{11}{}^p d_{12}^2 + k^2v^2(1-v)({}^m s_{11}{}^p d_{12}^2 + {}^m s_{11}{}^p d_{11}^2 - 2{}^m s_{12}{}^p d_{11}{}^p d_{11})\}.\end{aligned} \tag{2.9}$$

Amongst all the cases presented so far, the in-plane ME coefficient is expected to be the largest. This is due to availability of magnetostrictive and piezoelectric phases with high q- and d-values, respectively; and, to the absence of demagnetization fields. We will further use these outcomes later in the estimation of ME parameters for some specific examples.

2.2 Bilayer Structure

Theoretical modeling of low frequency ME effect described above is based on the homogeneous longitudinal strain approach. However, configurational asymmetry of a bilayer implies bending the sample in applied magnetic or electric field and variation in ME response. One of the principal objective of present section is modeling of the ME interaction in a magnetostrictive-piezoelectric bilayer taking into account the flexural strains (Petrov et al. 2009). We calculated ME voltage coefficients α_E for transverse field orientations to provide minimum demagnetizing fields and maximum α_E.

The thickness of the plate is assumed small compared to remaining dimensions. We assume the longitudinal axial strains of each layer to be linear functions of the vertical coordinate z_i to take into account bending the sample. To preserve force equilibrium, the axial forces in the three layers add up to zero, that is,

$$F_{p1} + F_{m1} = 0 \tag{2.10}$$

where $F_{i1} = \int_{-{}^{i}t/2}^{{}^{i}t/2} {}^{i}T_1 \, dz_1$.

The moment equilibrium condition has the form:

$$F_{m1} h_m = M_{m1} + M_{p1}, \tag{2.11}$$

where $M_{i1} = \int_{-{}^{i}t/2}^{{}^{i}t/2} z_i^i T_1 \, dz_1$.

Simultaneous solving (2.8) and (2.10) enables finding the axial stress components in the piezoelectric layer ${}^{p}T_1$ and ${}^{p}T_2$. Then the expression for ME voltage coefficient can be expressed using the open circuit condition

$$\alpha_{E,31} = \frac{E_3}{H_1} = -\frac{{}^{p}d_{31} \int_{-{}^{p}t/2}^{{}^{p}t/2} \left({}^{p}T_1 + {}^{p}T\right)_2 dz}{t \, H_1 {}^{p}\varepsilon_{33}},$$

where $t = {}^{m}t + {}^{p}t + {}^{s}t$ is the total thickness of considered structure.

Using the 1-D approximations of (2.1)–(2.10) enables one to obtain an explicit form of expression for ME voltage coefficient

$$\alpha_{E,31} = \frac{\left[\left(1-{}^{p}K_{31}^{2}\right){}^{p}s_{11}+{}^{m}s_{11}{}^{p}t^{3}/{}_{m}t^{3}\right]{}^{m}q_{11}{}^{p}d_{11}/{}_{p}\varepsilon_{33}}{{}^{p}s_{11}\left(1-{}^{p}K_{31}^{2}\right)\left[2^{p}t/{}_{m}t{}^{m}s_{11}\left(2+3^{p}t/{}_{m}t+2^{p}t^{2}/{}_{m}t^{2}\right)+\left(1-{}^{p}K_{31}^{2}\right){}^{p}s_{11}\right]+{}^{m}s_{11}^{2}{}^{p}t^{4}/{}_{m}t^{4}} \tag{2.12}$$

In case of neglecting the flexural strains, it is easily shown that expression for ME voltage coefficient reduces to well-known expression of Sect. 2.1 which was obtained with the assumption of homogeneous longitudinal strains.

2.3 Examples of Multilayer Structures

The preceding comprehensive theoretical treatment resulted in expressions of the ME voltage coefficients for three different orientations of fields, which were the ones of most importance, including: longitudinal, transverse, and in-plane longitudinal. The most significant features of the model are as follows: (i) Consideration of three different field configurations. This allows for the determination of a single-valued interface parameter k, facilitating quantitative characterization of the bilayer interface. (ii) Consideration of a new field configuration, i.e., in-plane longitudinal fields that has very strong ME coupling. And, (iii) consideration of the effect of a finite magnetic permeability on the magnetostriction of the magnetic subsystem: which was ignored in prior investigations.

Next, we apply the theory for the calculation of ME coupling in layered composites. Consider the materials couple cobalt ferrite and lead zirconate titanate (CFO–PZT), which is a system that has been of significant prior interests. Since the value of α_E depends notably on the concentration of the two phases, the ME voltage coefficient has been determined as a function of the volume fraction v of the piezoelectric phase in composite. Material parameters used for estimates are given in Table 2.1. Results of calculations using the model are illustrated in Fig. 2.2, which were obtained by assuming an ideal interface coupling ($k = 1$).

Results of $\alpha_{E,31}$ versus PZT volume fraction reveals a double maximum that is due to fact that the strain produced by the ferrite consists of two components: longitudinal and flexural. For a symmetric structure such as trilayer, there are no flexural strains and the maximum ME coefficient occurs for $V = 0.6$ (Bichurin et al. 2003). Since the flexural strain is opposite in sign compared to longitudinal one and reaches its maximum value for $V = 0.6$, the two types of strains combine to produce suppression of $\alpha_{E,31}$ at $V = 0.6$ and a double maximum in the ME coefficient as in Fig. 2.2. In what follows, we consider theoretical models of low frequency ME coupling for symmetric structures taking into account that such structures result in higher values of ME coefficients.

The variation of $\alpha_{E,33}$ with v for various values of coupling parameter k is shown in Fig. 2.3a for a symmetric structure which excludes the flexural deformations. The magnitude of $\alpha_{E,33}$ decreases with decreasing k, and $v_{\max}$ shifts to

Table 2.1 Material parameters (compliance coefficient s, piezomagnetic coupling q, piezoelectric coefficient d, and petmittivity ε) for lead zirconate titanate (PZT), cobalt ferrite (CFO), and lanthanum strontium manganite used for theoretical values

Material	s_{11} (10^{-12} m^2/N)	s_{12} (10^{-12} m^2/N)	s_{13} (10^{-12} m^2/N)	s_{33} (10^{-12} m^2/N)	q_{33} (10^{-12} m/A)	q_{31} (10^{-12} m/A)	d_{31} (10^{-12} m/V)	d_{33} (10^{-12} m/V)	$\varepsilon_{33}/\varepsilon_0$
PZT	15.3	−5	−7.22	17.3	–	–	−175	400	1,750
CFO	6.5	−2.4			−1,880	556	–	–	10
LSMO	15	−5			250	−120	–	–	10

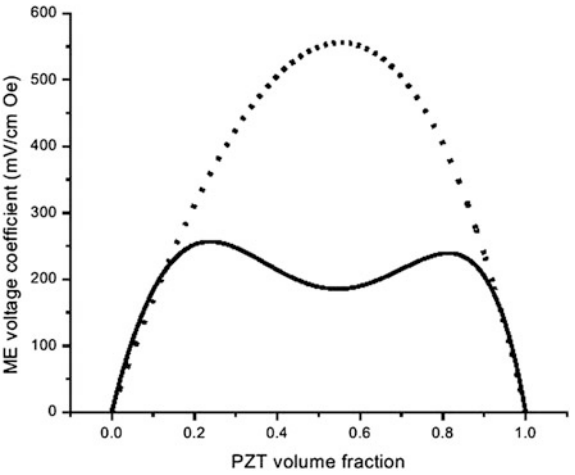

Fig. 2.2 PZT volume fraction dependence of transverse ME voltage coefficient $\alpha_{E,31} = \delta E_3/\delta H_1$ for a perfectly bonded ($k = 1$) bilayer (*solid line*) and symmetric structure (*dot line*) of CFO and PZT

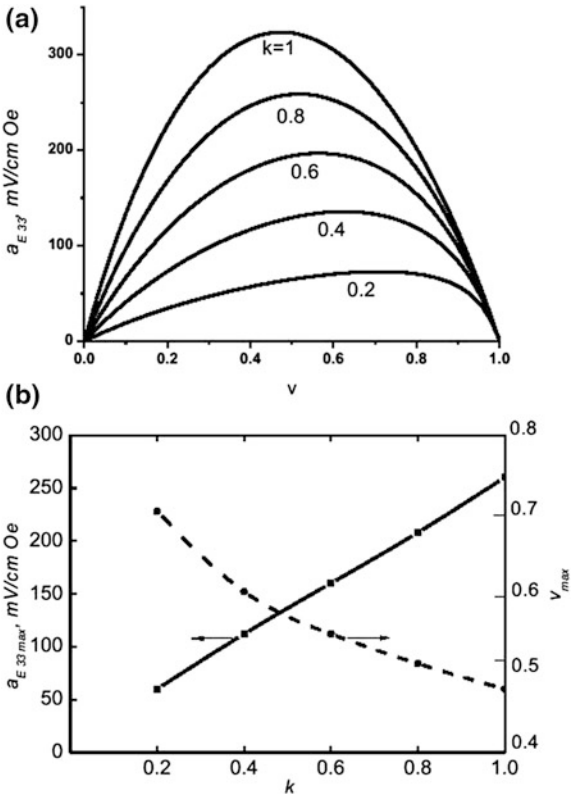

Fig. 2.3 **a** Estimated dependence of longitudinal ME voltage coefficient on interface coupling k and volume fraction v for symmetric structure of CFO and PZT. **b** Variation with k of maximum $\alpha_{E,33}$ and the corresponding $v_{\max}$

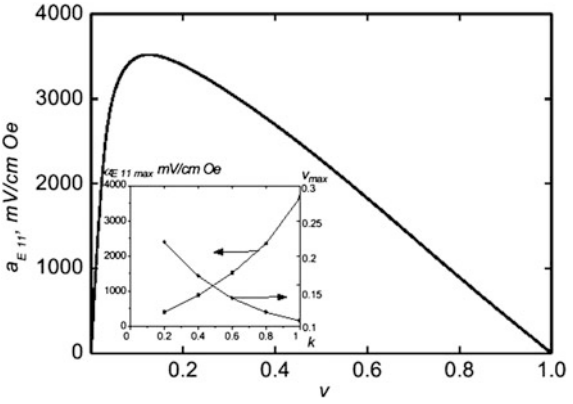

Fig. 2.4 ME voltage coefficient for a perfectly bonded (k = 1) symmetric structure of CFO and PZT for in-plane longitudinal field orientation. The poling field and dc and ac magnetic and electric fields are in the sample plane and parallel to each other. *Inset* shows variation of maximum $\alpha_{E,33}$ and the corresponding v_{max} with k

PZT-rich compositions. Figure 2.3b shows the dependence of the maximum value in $\alpha_{E,33}$ on k, where calculations are illustrated for various values of v_{max}. With increasing k, a near-linear increase was found in the maximum value of $\alpha_{E,33}$. For transverse fields, the maximum α_E is 40 % higher than that of $\alpha_{E,33}$. This is due to the strong parallel piezomagnetic coupling q_{11} which determines α_E, relative to that of q_{31} which determines $\alpha_{E,33}$.

Next, we consider the ME effect in CFO–PZT for the in-plane longitudinal field orientation.

The most significant prediction of the present model is that the strongest ME coupling should occur for in-plane longitudinal fields, as shown in Fig. 2.4. One can easily see in Fig. 2.4 that when the field is switched from longitudinal to in-plane longitudinal that the maximum value of the relevant ME coefficient increases by nearly an order of magnitude: $\alpha_{E,max} = 325$ mV/cm Oe for the longitudinal orientation, whereas $\alpha_{E,11} = 3{,}600$ mV/cm Oe for the in-plane longitudinal. The v-dependence of $\alpha_{E,\,11}$ reveals a rapid increase in the ME coefficient to a maximum value of $\alpha_{E,11} = 3{,}600$ mV/cm Oe for $v = 0.11$, which is followed by a near-linear decrease with further increase of v. Such an enhancement in the in-plane longitudinal coefficient relative to the longitudinal one is understandable due to (i) the absence of demagnetizing fields in the in-plane configuration, and (ii) increased piezoelectric and piezomagnetic coupling coefficients compared to longitudinal fields. The down-shift in the value of v_{max} (from 0.5 to 0.6 for longitudinal and transverse fields to a much smaller value of 0.1) is due to the concentration dependence of the effective permittivity.

Another layered structure of importance is nickel ferrite (NFO)–PZT. Although NFO is a soft ferrite with a much smaller anisotropy and magnetostriction than CFO, efficient magneto-mechanical coupling in NFO–PZT gives rise to ME voltage coefficients comparable to those of CFO–PZT. Using the model presented in this chapter, we can estimate α_E for NFO–PZT for different field orientations and conditions, similar to that for CFO–PZT.

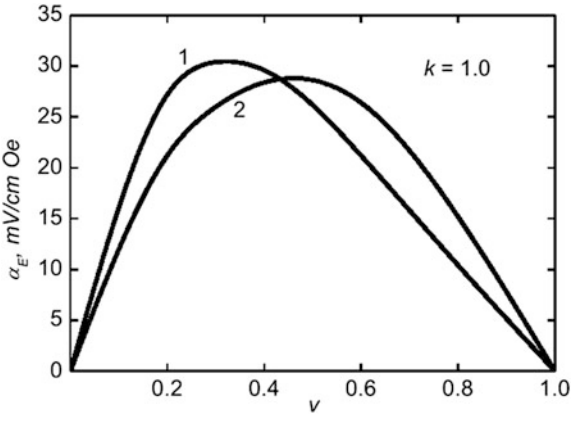

Fig. 2.5 *1* Longitudinal and *2* transverse ME voltage coefficients as functions of PZT volume fraction for symmetric layered structure of $La_{0.3}Sr_{0.7}MnO_3$ (LSMO) and PZT for interface coupling parameter k =1

Finally, we consider composites that have lanthanum strontium manganites for the magnetostrictive phase. Lanthanum manganites with divalent substitutions have attracted considerable interest in recent years due to double exchange mediated ferromagnetism, metallic conductivity, and giant magnetoresistance. The manganites are potential candidates for ME composites because of (i) high magnetostriction and (ii) metallic conductivity that eliminates the need for a foreign electrode at the interface. Figure 2.5 shows the longitudinal and transverse ME voltage coefficients for unclamped $La_{0.3}Sr_{0.7}MnO_3$ (LSMO)–PZT laminate that assumes ideal coupling at the interface and no bending strain. In this case, the values of the ME coefficients are quite small compared to that of ferrite–PZT: this is due to weak piezomagnetic coefficients and compliances parameters for LSMO. The ME coefficient for in-plane longitudinal fields and the effects of clamping for different field orientations were similar in nature to those for ferrite–PZT layered structure, and thus are not discussed in any detail here.

It is important to compare the theoretical predictions, illustrated above, with experimental data. Let us consider first a bilayer of CFO–PZT taking into account the flexural deformations. Figure 2.6 shows α_E as a function of v. These data were obtained at low frequencies (100–1,000 Hz). The desired volume fractions v was achieved by careful control of the layer thickness. Data show an increase in α_E with v until a maximum is reached. However, these data clearly demonstrated that the actual experimental value is an order of magnitude smaller than that predicted in Figs. 2.2 and 2.3 (assuming $k = 1$). It is, therefore, reasonable to compare the data with calculated values of α_E as a function of v using a reduced interface coupling parameters of $k = 0.1$: in this case, agreement between theory and experiment can be seen, as shown in Fig. 2.6. The key inference that can be made concerns the inherently poor interface coupling for CFO–PZT, irrespective of sample synthesis techniques. We address possible causes for this poor coupling later in this section.

A third materials couples, LSMO–PZT, is considered in Fig. 2.7, which shows α_E as a function of v for longitudinal and transverse fields. The α_E values are the

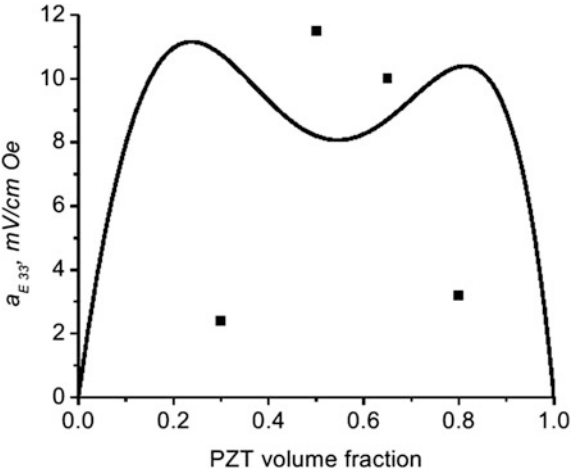

Fig. 2.6 PZT volume fraction dependence of longitudinal ME voltage coefficient of CFO–PZT bilayer. Solid line are theory for $k = 0.1$ and points are experiment

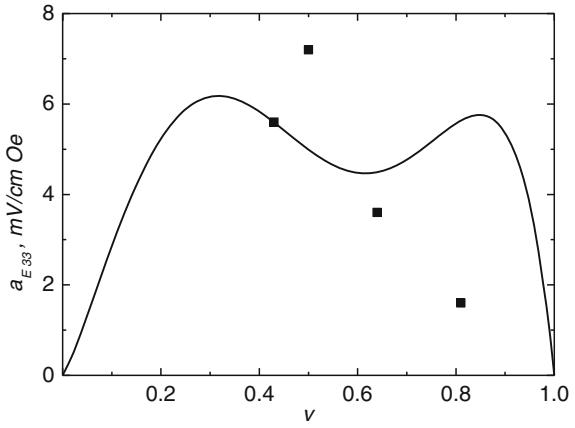

Fig. 2.7 PZT volume fraction dependence of transverse **a** and longitudinal **b** ME voltage coefficients for LSMO–PZT bilayer: *solid lines* are the theory for $k = 0.2$ and points are experiment

smallest amongst the three systems considered here. Calculated values assuming $k = 1$ were found to be quite high compared to the data, rather it was found that nonideal values of $k = 0.2$ gave reasonable agreement with the data. Thus, one can readily infer poor interfacial coupling in LSMO–PZT, similar to that for CFO–PZT.

Finally, we should comment on a possible cause of poor interfacial coupling for CFO–PZT and LSMO–PZT, and ideal coupling for NFO–PZT. The parameter k can be expected to be sensitive to mechanical, structural, chemical, and electromagnetic parameters at the interface. We attribute unfavorable interface conditions in CFO–PZT and LSMO–PZT to inefficient magneto-mechanical coupling. The magneto-mechanical coupling k_m is given by $k_m = (4\pi\lambda'\mu_r/E)^{1/2}$; where λ' is the dynamic magnetostrictive constant and μ_r is the reversible permeability, and E is Young's modulus. In ferrites, under the influence of a dc magnetic bias H and

ac magnetic field δH, domain wall motion and domain rotation contribute to the Joule magnetostriction and consequently to the effective linear piezomagnetic coupling. A key requirement for strong coupling is unimpeded domain wall motion and domain rotation. A soft ferrite with a high initial permeability (i.e., low anisotropy), such as NFO, will have key materials parameters favoring a high k_m, and consequently, strong ME effects. Measurements have shown that NFO has an initial permeability of 20, whereas that of LSMO and CFO is 2–3. Thus, one can infer a plausible simple explanation of the near interfacial parameter for NFO–PZT is (in part) favorable domain motion.

In deriving the above expression, we assumed the electric field to be zero in magnetic phase since magnetostrictive materials that are used in the case under study have a small resistance compared to piezoelectric phase. Estimate of ME voltage coefficient for CFO–PZT layered structure gives $\alpha_{E,\,33} =$ 325 mV/cm Oe providing that the bending strains are ignored. However, considering CFO as a dielectric results in $\alpha_{E,\,33} = 140$ mV/cm Oe (Osaretin and Rojas 2010) while the experimental value doesn't exceed 74 mV/cm Oe (Harshe et al. 1993). We believe CFO should be considered as a conducting medium compared to dielectric PZT in the low-frequency region in accordance with our model. The discrepancy between theoretical estimates and data can be accounted for by features of piezomagnetic coupling in CFO and interface coupling of bilayer (Bichurin et al. 2003).

2.4 Bulk Composites

Design of new ME composites assumes the use of reliable theoretical models, allowing prediction of properties for various materials couples and over a range of laminate parameters. Manufacturing methods of all-ceramic composites are based on an initial mixing of starting powders batched in proportion to the composite volume fraction, followed by pressing and densification/sintering to a net-shape. Clearly, if the concentration of one of the constituent phases is small, then that phase will consist of isolated particles in a matrix. Following accepted classification nomenclature (Newnham et al. 1978) this composite should be referred to as a 0–3 type, as one phase is isolated (i.e., connected in zero dimensions) and the second is interconnected in three dimensions. If the volume fraction of the secondary phase in the matrix is increased, and a percolation limit is reached, then it is classified as a 1–3 type composite. If the secondary phase then crosses that initial percolation limit, and subsequently begins to be interconnected in two dimensions, the composite connectivity is known as the 2–3 type. We mention these things at this time to make the point that the same ceramic manufacturing technology allow the fabrication of a wide range of relative volume fractions of the different phases in an all-ceramic composite, and consequently to various possible types of dimensional interconnectivities. Accordingly, it is very important to choose the

correct method of calculation for effective constants of a composite at various relative volume fractions of components.

Unfortunately, exact solutions of three-dimensional problems related to the calculation of effective constants of inhomogeneous systems are unknown. Therefore, there is presently no precise structural classification of composites. Within the limited theory of heterogeneous systems of two-phase composites, there are two principle approaches to approximate solutions: matrix systems and two-component mixtures, for which behavior of effective parameters depending on concentration continuously.

In the case of matrix systems, modification of the concentration from 0 to 1 does not change the qualitatively structure of the composite: at any concentration, one of the components must form a coherent matrix that contains isolated particles of the second component. The system always remains essentially non-central, and matching formulas for an evaluation of effective constants give their continuous dependence on concentration in the entire range from 0 to 1. We should note that the application of these formulas to the calculation of effective constants of composites is not always justified.

The case of two-component mixtures is characterized by a qualitative modification of the structure of the composite, as the concentration is changed. Such systems are characterized, as is well known, by critical concentrations at which point there are important property changes such as metal–insulator or rigid-plastic transformations. The metal–insulator transformation occurs in a composite consisting of an insulating and conductive phases. Assume that the insulating phase is initially the matrix and that the conductive one consists of isolated particles. In this case, initially the composite is insulating; however, when the percolation limit is crossed, the conducting particles form an interconnected conduction pathway, dramatically lowering the resistivity near a critical volume fraction. In the second example (rigid-plastic transformation), it is supposed that the composite is a mixture in which the elastic compliance of one of the constituent phases tends to infinity (for example, a porous composite). This composite type posses a critical concentration of the second phase, above which the rigid framework of the composite loses its stability. It should be straightforward to see that any bulk composites will have numerous effective materials properties, all of which change with relative phase volume fraction from in a manner independent of other properties.

As an example, we consider a composite with a 3–0 type connectivity. Cubic models for ferrite–ferroelectric composites with a connectivity of 3–0 and 0–3 have been considered by Harshe et al. (1993). Numerically, the ME coefficient is equal to the ratio of the electric field induced on the composite by an applied magnetic field: the ME coefficient is equal to E_3/H_3. It is necessary to realize that the magnetic field was applied only to the ferrite phase: i.e., $E_3/{}^{m}H_3$ where ${}^{m}H_3$ is the local magnetic field on the ferrite phases which may exceed that applied to the entire composite. Harshe's study only considered the case of free cubic cells, and effective parameters of the composite in known model systems were not

determined. However, in real composites, we must consider the case of non-free cells. It is also very important to use any such model to predict the effective composite parameters. In the following section, we present a generalized model for ferrite–piezoelectric composites that allows one to define and predict the effective parameters of said composite using given conditions.

The properties of this ME composite will depend on the parameters of the corpuscles, and also on the terminal conditions. Now, let us suppose that the geometrical model for ME composites in this figure is miniaturized to fine scales. If the given cubic model ME composite is considered as a material consisting of consecutive and parallel connections of cubic cells with legs of unit length, then it is obvious by the definition of properties of a composite that it is possible to consider only one cubic cell rather than the entire ensemble of cells. The magnetostriction phase is enclosed by piezoelectric ones along different directions.

$$\begin{aligned} S_1 &= -s_{c1}s_{11}T_1, \\ S_2 &= -s_{c2}s_{22}T_2, \\ S_3 &= -s_{c3}s_{33}T_3, \end{aligned} \tag{2.13}$$

where $s_{ci} = {}^{c}s_{ii}/s_{ii}$ is the relative compliance of surroundings, and $c_{s_{ii}}$ is effective compliance of composite.

PZT volume fraction dependence of effective ME susceptibility is shown in Fig. 2.8 (Petrov et al. 2004, 2007).

The dependence of the effective ME voltage coefficient, defined as $\alpha_{E,33} = -\alpha_{33}/\varepsilon_{33}$, on the piezoelectric phase volume fraction can then be easily obtained, as shown in Fig. 2.9. These graphical solutions then allow one to determine the piezoelectric and magnetostrictive phase volume fractions that yield maximum values for the effective ME susceptibility (Fig. 2.8) and the ME voltage coefficient (Fig. 2.9).

The values of the ME voltage coefficient in Fig. 2.10 coincide with previously published data (Harshe et al. 1993), demonstrating the usefulness of the predictions. As follows from Fig. 2.10, the ME voltage coefficient was approximately 20 % greater than that calculated from the experimental data using the model. This is explained by the fact that the internal (local) magnetic field in the ferrite component is considerably different than that of the externally applied magnetic field.

Measurements of the ME voltage coefficient have been performed for bulk composites of NFO–PZT, using the experimental methodology mentioned above. Data are shown in Fig. 2.11 for the ME voltage coefficient as a function of the piezoelectric phase volume fraction. These measured values are much lower in magnitude than the theoretical ones predicted for the free composite condition. However, considering a clamped condition defined by the matching $s_{c11} = s_{c22} = s_{c33} = 0.3s_{33}$, agreement between theory and experiment was found, as illustrated in Fig. 2.11. These results indicate in real 0–3 ferrite–piezoelectric ceramic composites mixtures that the component phase grains are mechanically clamped by neighboring grains and by environmental boundary conditions.

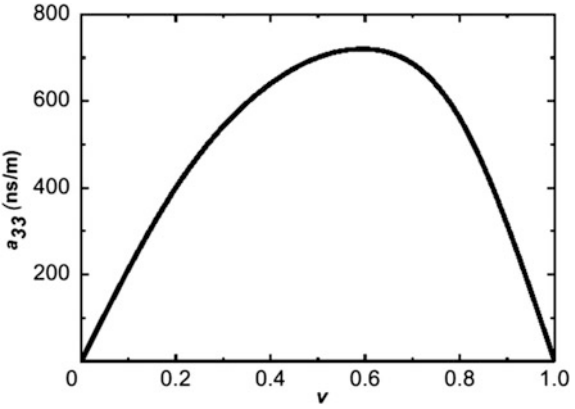

Fig. 2.8 PZT volume fraction dependence of ME susceptibility for CFO–PZT composite with connectivity 3–0

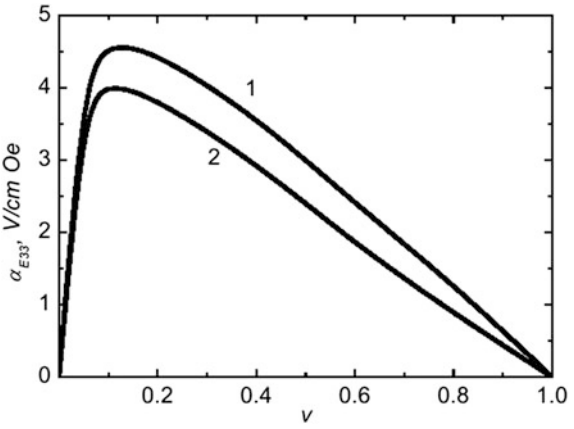

Fig. 2.9 PZT volume fraction dependence of ME voltage coefficient for CFO–PZT composite with connectivity 3–0 according to model (Petrov et al. 2004) *1* and model (Harshe et al. 1993) *2* for $\alpha_{E33} = E_3/^m H_3$ and material parameters from Table 2.1

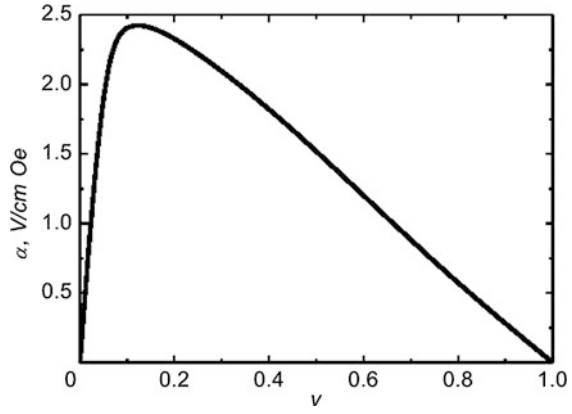

Fig. 2.10 Concentration dependence of $\alpha_{E33} = E_3/^m H_3$ for composite with material parameters from (Petrov et al. 2004)

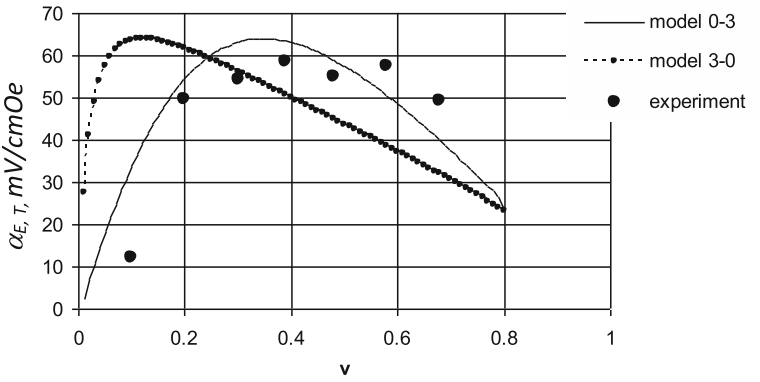

Fig. 2.11 ME effect in bulk composite of NFO and PZT

2.5 Magnetoelectric Effects in Compositionally Graded Layered Structures

A key drawback of functional devices based on ME materials is the need of prior polarization of ferroelectric phase and magnetic bias field of magnetic phase. Poling consists in heating the sample to Curie temperature and slow cooling in a static electric field. The bias magnetic field magnitude should correspond to maximal piezomagnetic coupling coefficient which provides the maximal ME coefficient. Thus supplementary constructional elements are necessary to provide poling and biasing the sample.

Here we prepare a composite based on magnetization-graded magnetic phase from compositionally graded ferromagnetic and polarization-graded piezoelectric phase from compositionally graded ferroelectric. Using the polarization-graded piezoelectric phase is known to result in a built-in static electric field. The amplitude of this field is determined by polarization gradient, $E_i = -\frac{1}{\varepsilon_0}\int_0^L \frac{\partial P}{\partial x}\,dx$ where L is the sample length. Analogously, magnetization gradient gives rise to a built-in static magnetic field, $H_i = -\frac{1}{\mu_0}\int_0^L \frac{\partial M}{\partial x}\,dx$. The above expressions show that the proper choice of polarization and magnetization gradients and sample length enables one to get the built-in electric and magnetic fields needed for obtaining the maximal piezoelectric and piezomagnetic coupling coefficients. It should be noted that there is no need in preliminary poling and magnetic biasing the sample (Petrov and Srinivasan 2008; Mandal et al. 2011).

As an example, we consider a magnetostrictive-piezoelectric bilayer of nickel–zinc ferrite and PZT. Bilayer includes the magnetic layer which is compositionally graded along the sample plane and the piezoelectric layer which is compositionally graded perpendicular to the sample plane. The output voltage induced by ME

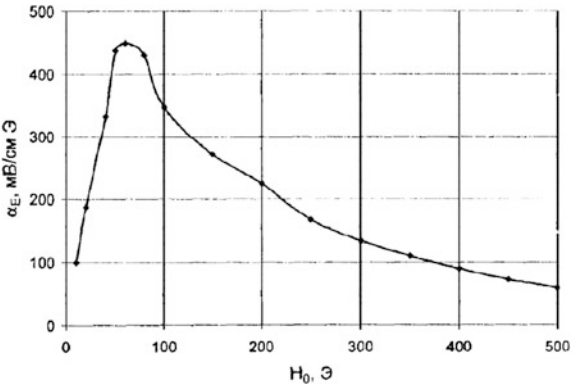

Fig. 2.12 Bias field dependence of ME voltage coefficient for bilayer of compositionally graded nickel–zink ferrite and PZT

coupling is measured across the sample thickness. Estimated bias field dependence of ME voltage coefficient is shown in Fig. 2.12 for equal volume fractions of ferrite and PZT.

Variation of zinc content from 0.3 to 0.5 gives rise to a magnetization gradient in the sample plane that results in a built-in magnetic field of 44 Oe. Estimates show that variation of zinc content from 0.3 to 0.5 enables one to increase the built-in magnetic field up to 60 Oe. Figure 2.12 shows that bias field of 60 Oe provides obtaining ME voltage coefficient of 450 mV/cm Oe.

2.6 Magnetoelectric Effect in Dimensionally Graded Laminate Composites

Dimensionally gradient piezoelectric plate with thickness of 1 mm was fabricated by mechanical polishing and dicing technique, as shown in Fig. 2.13a (Park et al. 2012). Piezoelectric plates with composition $Pb\left(Zn_{1/3}Nb_{2/3}\right)_{0.2}(Zr_{0.5}Ti_{0.5})_{0.8}O_3$ [PZNT] were synthesized by conventional mixed oxide method. Piezoelectric constant of poled PZNT plates was found to be 500 pC/N and the dielectric constant was 2,219 at 1 kHz. The piezoelectric voltage constant (g_{33}) was of the order of 23.41×10^{-3} Vm/N. On this PZNT plate, 25 μm-thick Metglas (2605SA1, Metglas Inc, USA) sheets of desired dimensions were attached using epoxy (West System, USA) with the curing temperature of 80 °C. Impedance spectrum of the composites was measured by LCR meter (HP 4194A). For ME voltage coefficient measurement in longitudinal–transversal (L–T) mode configuration, an electromagnet was used to apply the DC magnetic field and the samples were placed in the center of the Helmholtz coil under an AC magnetic field (H_{ac}). The voltage induced on the laminate was monitored by using a lock-in amplifier. The magnetostriction was evaluated by using the strain gauge and Wheatstone bridge.

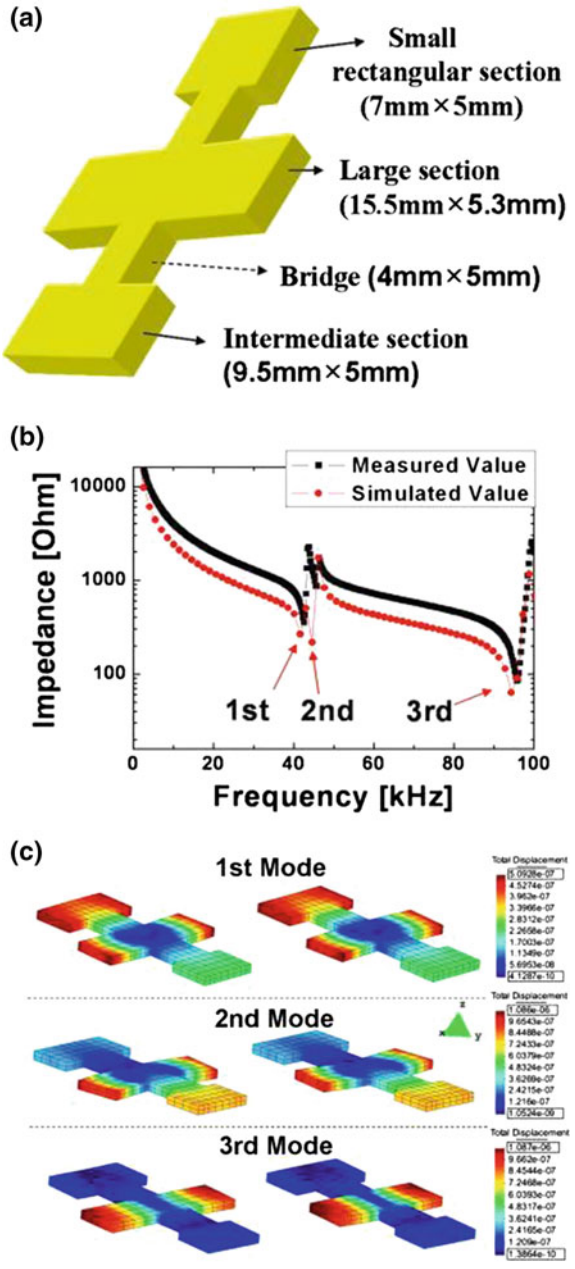

Fig. 2.13 **a** Schematic diagram of asymmetric piezoelectric plate, **b** impedance spectrums from simulation and measurement, and **c** resonance displacements at 42, 44, and 94.3 kHz

Impedance spectrum of asymmetric piezoelectric plate was measured to identify the EMR range. The first, second, and third resonances were found to be 42, 44, and 94.3 kHz, respectively. In comparison, measured impedance spectrums for

the asymmetric piezoelectric plate exhibited resonance peaks at 42, 44, and 96 kHz, as shown in Fig. 2.13b. Thus, the results between simulation and measurement were in good agreement. The first mode at 42 kHz was associated with biaxial bending of the large rectangular section and the intermediate rectangular section, while the second mode at 44 kHz was related to the biaxial bending of the large rectangular section and the small rectangular section. The third mode at 99 kHz came from the lateral displacement of the large rectangular section, as shown in Fig. 2.13c.

Figure 2.14a shows the fabricated ME laminate composite based on Fig. 2.13a. On top of the PZNT layer, four layers of Metglas with the area of 13×7 mm^2 were attached at the middle rectangular section (Section A), 30 layers of Metglas with area of 20×7 mm^2 were attached at the larger rectangular section (Section B), and five layers of Metglas with area of 7×7 mm^2 were attached at the intermediate rectangular section (Section C), as shown in Fig. 2.14a. There are two variables which could be adjusted to achieve a wideband ME response. First, if the rectangular area of two sections in piezoelectric plate is different than the one with smaller number of Metglas layers will show higher ME coefficient. Second, if the numbers of Metglas layers are same, the rectangular section with the smaller area will show smaller ME coefficient. Thus, by adjusting the ratio of Metglas layers on various rectangular sections, a composite ME response with flat behavior can be obtained.

Figure 2.14b shows the magnetostriction (S_{ij}) and piezomagnetic (q_{ij}) coefficient for varying dimensions and stack configurations of Metglas. In this figure, S_{11} corresponds to longitudinal in-plane magnetostriction parallel to H_{DC} and q_{11} is the longitudinal in-plain piezomagnetic coefficient corresponding to the differential of S_{11}. The maximum in-plane magnetostriction was found to be 28 ppm regardless of Metglas stack configurations and dimensions; however, the strain behavior was strongly dependent on the stack configuration and dimensions. Four layers of Metglas with the area of 13×7 mm^2, 30 layers of Metglas with area of 20×7 mm^2, and five layers of Metglas with area of 7×7 mm^2 showed piezomagnetic coefficient corresponding to 0.38, 0.21, and 0.16 ppm/Oe at 70, 150, and 204 Oe of H_{DC}, respectively. These piezomagnetic behaviors will result in strong elastic coupling with the piezoelectric sections.

Figure 2.14c shows the measured ME response from the composite structure as a function of magnetic DC bias under the condition of $H_{AC} = 1$ Oe at $f = 1$ kHz. The peak at 70 Oe was associated with section A. The second peak of the ME coefficient at 150 Oe was associated with section C. The third peak of the ME coefficient at 209 Oe was associated with section B. The value of DC bias at the peak in piezomagnetic coefficient corresponds to that for the peak in ME coefficient. Further, it was found that not only piezomagnetic coefficient but also piezoelectric dimensions affected elastic coupling between the Metglas and piezoelectric sections compared to Fig. 2.14b and c. Furthermore, if only section A and section B were combined, there will be a valley in the intermediate range. By inserting section C, the formation of flat ME band was facilitated. The overall ME

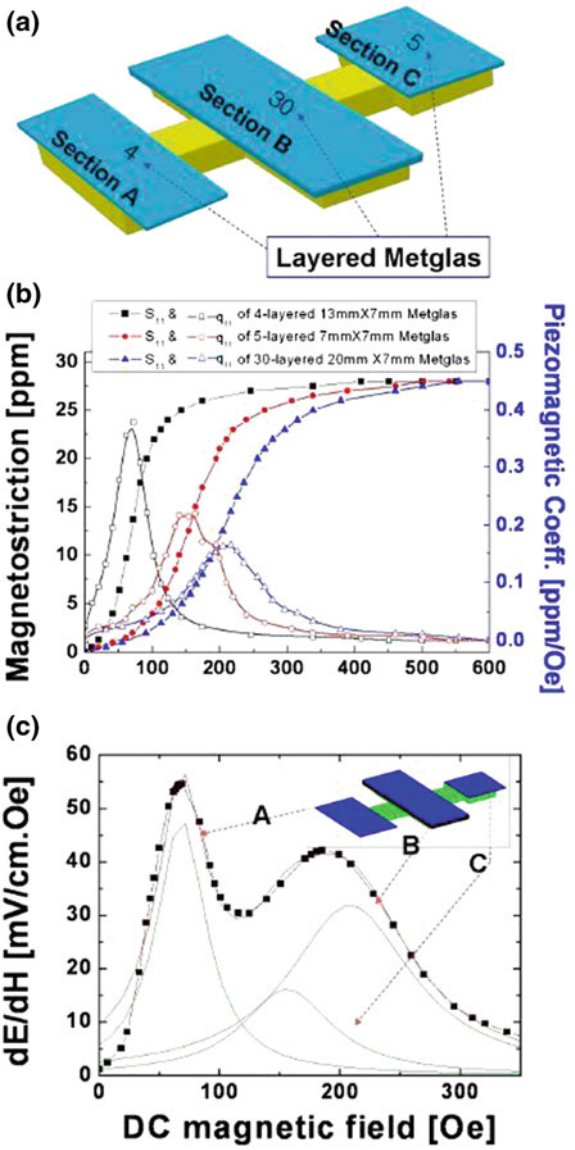

Fig. 2.14 **a** Schematic diagram of laminated ME composite, **b** magnetostriction (S_{11}) and piezomagnetic coefficient (q_{11}) for varying dimensions and stack configurations of Metglas, **c** ME response as a function of DC magnetic field under the constant condition of $H_{ac} = 1$ Oe at $f = 1$ kHz

response as a function of magnetic DC bias was composite of three individual responses.

The impedance and phase angle spectrums for this laminate are shown in Fig. 2.15a. After Metglas was attached on the PZNT plate, multiple resonances occurred at 14, 28, 41, 44, and 107 kHz as marked with arrows in Fig. 2.15a. Resonant modes at 14 and 28 kHz were found to be related to the bending vibrations of all the sections. The middle section dominated the vibration mode at

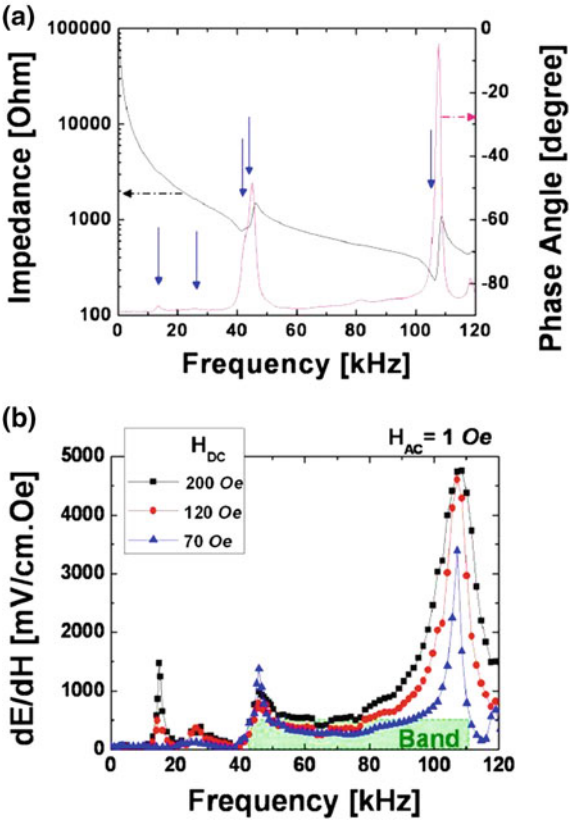

Fig. 2.15 **a** Impedance and phase angle spectrums of the ME composite, **b** ME response as a function of frequency

14 kHz while the small rectangular section dominated the vibration mode at 28 kHz. The resonance at 41 kHz was found to be combination of the bending motions of large rectangular section (section B) and middle rectangular section (section A). The resonance at 44 kHz was related to combined bending response from the bridge and small rectangular section (section C). The resonant modes of ME composite at 41 and 44 kHz were correlated to the first and second resonance modes of PZNT layer as determined in Fig. 2.13b. The resonant mode at 107 kHz had a similar vibration mode as that at 44 kHz.

The ME output voltage from composite was measured as a function of frequency under constant $H_{AC} = 1$ Oe but varying $H_{DC} = 70$, 120, and 200 Oe, as shown in Fig. 2.15b. Interestingly, ME response as a function of frequency had similar behavior as that of phase angle shift shown in Fig. 2.15a and b. The ME peaks are shown at 14, 28, 45, and 107 kHz corresponding to the resonance frequencies observed in the impedance measurement. The peak ME response at 45 kHz was associated with resonances at 41 and 44 kHz. The maximum ME coefficient was found to be 4,740 mV/cm Oe at $f = 107$ kHz under $H_{DC} = 200$ Oe. Interestingly, the bands were successfully formed in the range of

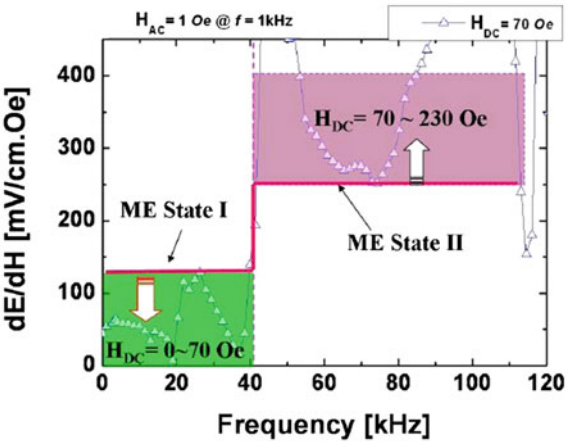

Fig. 2.16 Schematic of switchable ME response dependency on the frequency and DC magnetic field conditions

41–110 kHz. The composite showed high ME coefficient of 260 mV/cm Oe after the resonance peak of 41 kHz, regardless of the applied DC magnetic field. These widely extended bands were derived from the combination of the resonances at 41, 44, and 107 kHz.

The maximum ME coefficients of 1,400 and 4,740 mV/cm Oe was found at 45 and 107 kHz respectively. The band at 107 kHz exhibited ME coefficient higher than 3,000 mV/cm Oe from 52 to 242 Oe of H_{DC} while the band at 45 kHz exhibited ME coefficient higher than 780 mV/cm Oe from 40 to 230 Oe of H_{DC}. The bands were obtained regardless of applied DC and AC magnetic fields. The wideband was formed in both conditions of the frequency range of 41–110 kHz and DC magnetic ranges of 40–230 Oe and 52–242 Oe at $f = 45$ and 107 kHz, as shown in Figs. 2.15b.

Interestingly, there are two noticeable states in the ME frequency response in Fig. 2.15b. Under the constant DC magnetic field condition of 70 Oe, the composite showed flat ME responses in both frequency ranges of 1–11 kHz (state I) and 41–110 kHz (state II) as shown in Fig. 2.16. Figure 2.16 shows the schematic diagram of resulting ME response as a function of frequency and the applied DC magnetic field conditions. State I shows a band lower than 129 mV/cm Oe before $f = 41$ kHz while State II shows a band higher than 260 mV/cm Oe after $f = 41$ kHz under the constant condition of $H_{DC} = 70$ Oe. The ME coefficient of State II was 2× higher than that of State I. Consequently, ΔME (=$ME_{StateII}$ − ME_{StateI}) was 131 mV/cm Oe under the constant $H_{DC} = 70$ Oe. These states were found to be adjustable with changing H_{DC} conditions. The maximum value of the ME_{StateI} can be reduced by decreasing the DC magnetic field and ranges between 0 and 129 mV/cm Oe. On the other hand, the minimum value of the $ME_{StateII}$ can be elevated by increasing DC magnetic field condition in the range of 260–406 mV/cm Oe. Thus by tuning the frequency and H_{DC} ΔME in the range of 131 and 406 mV/cm Oe can be achieved which clearly shows the tunability of this device.

These signals are strong enough to allow two distinguishable states. The clear sensing margin was seen between state I and state II: the ME values in state II were at least two times higher than that in state I. This interesting and promising ME behavior can be exploited in several applications. The wideband behavior can be a candidate for magnetic field controlled switches as well as ME harvesters. In the case of the magnetic field-controlled switches, the resonant frequency becomes the cut-off condition and the state I and state II can be considered as "off" and "on," respectively.

We attempt to model the response of the laminate structure by calculating the in-plane strain and stress components for all sections and at the end combining them together to find the overall solution. The total vibration spectrum of the laminate composite consists of several contributions. The first mode is supposed to be associated with simultaneous bending vibrations of the small rectangular section with its bridge and the middle rectangular section. The equation of bending motion of *i*th-area (1 and 2 areas correspond to bridge and section) has the form:

$$\nabla^2\nabla^2 w_i + \frac{\rho_i\, t_i}{D_i}\frac{\partial^2 w_i}{\partial t^2} = 0, \tag{2.14}$$

where $\nabla^2\nabla^2$ is biharmonic operator, w_i is the displacement in z-direction, t_i is thickness, ρ_i is average density of *i*-area, and D_i is cylindrical stiffness. The strain's components can be expressed in terms of displacement as $S_{1i} = -z\frac{\partial^2 w_i}{\partial x^2}$ and $S_{2i} = -z\frac{\partial^2 w_i}{\partial y^2}$. The stress components can be expressed in terms of strains as:

$$\begin{aligned} \left({}^{p}S_k\right)_i &= {}^{p}s_{kj}\left({}^{p}T_j\right)_i + {}^{p}d_{31}{}^{p}E_{3i}; \\ \left({}^{m}S_k\right)_i &= {}^{m}s_{kj}\left({}^{m}T_j\right)_i + \left({}^{m}g_{k1}\right)_i^{m}B_{1i}; \end{aligned} \tag{2.15}$$

where S_{1i} and T_{1i} are strain and stress components for *i*-area, E_{3i} is the component of electric field, H_{1i} is the component of magnetic field, s_{kj}, is compliance at constant electric field for piezoelectric and at constant magnetic induction for magnetic component, g_{k1} and d_{31} piezomagnetic and piezoelectric coefficients correspondingly. The superscripts p and m correspond to piezoelectric and piezomagnetic layers. Solving (2.14) for displacement of each section by using the boundary conditions given below provides the dynamic solution: $w_1 = 0$ and $\partial w_1/\partial x = 0$ at $x = 0, w_1 = w_2, \partial w_1/\partial x = \partial w_2/\partial x, (M_1)_1 = (M_1)_2$ and $(V_1)_1 = (V_1)_2$ on the boundary of 1 and 2-areas; $(M_1)_2 = 0$ and $(V_1)_2 = 0$ at $x = L$ (L is the total length of section and bridge); $(M_2)_i = 0$ and $(V_2)_i = 0$ at $y = \pm b_i/2$ (b_i is the width of *i*-area), where $(M_j)_i$ is the moment of rotation and $(V_j)_i$ is the transverse force with respect to j-axis.

The computed displacements were used to determine the strain components and then the stress components from (2). Substituting the stress components into open circuit condition enables the calculation of the ME voltage coefficient by taking into account condition that average electric field induced across the piezoelectric

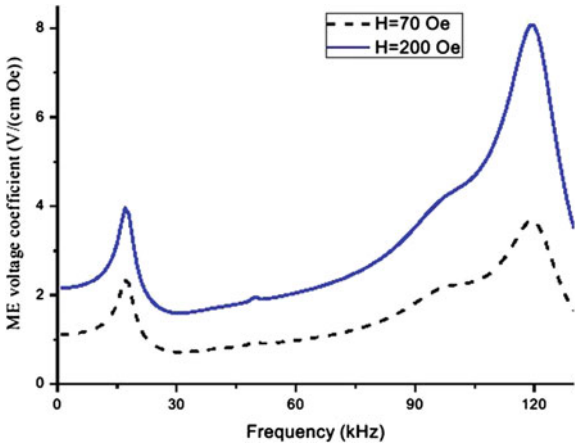

Fig. 2.17 Frequency dependence of ME voltage coefficient for Metglas—PZNT composite for bias field of 200 and 70 Oe

layer is estimated as integral of internal electric field taken over the piezoelectric thickness, $E = \frac{1}{t_p}\int_{t_p} {}^{p}E_3\, dz$. These calculations were carried out numerically. The resonance frequencies for the small rectangular section and the middle rectangular section were found to be approximately equal. The second harmonic of this mode can be seen at 97 kHz. It should be noted that theoretical estimate for the next resonance frequency (at 44 kHz) as the bending mode of large rectangular section was made using similar procedure. The bridge was not included into vibrating system since its displacement (in z direction) was negligible. Finally, the mode at 120 kHz was calculated under assumption that it came from the axial mode of the large rectangular section. The estimate for this case was found using the computing method known heretofore.

Figure 2.16 shows that the first mode at 17 kHz can be associated with simultaneous bending vibrations of the small rectangular section and the middle rectangular section, while the second mode at 44 kHz can be related to the bending of the large rectangular section. The third peak corresponds to second harmonic of first mode and occurs at 97 kHz. The fourth mode at 120 kHz came from the axial mode of the large rectangular section. Figure 2.16 reveals a frequency band of 90–130 kHz which is dependent on dc magnetic field. This band arises from the combination of the resonances. One can see two states in the ME frequency response at 70 Oe. The ME response in the frequency ranges of 25–90 kHz (state I) and 90–130 kHz (state II) is shown to be a function of frequency and the applied DC magnetic field. State I corresponds to a band lower than 1.8 V/cm Oe while State II shows a band higher than 1.8 V/cm at bias field of 70 Oe. These states are adjustable with changing H_{DC}. Some disagreement between estimates and data can be accounted for by distinctions between the geometry of actual composite structure and that of simple model used for obtaining the estimates.

Thus, we demonstrate a ME resonator exhibiting wideband behavior by fabricating a dimensionally gradient structure and combining with laminate configuration. We were able to obtain a flat ME response in the DC magnetic bias range

of 52–242 Oe where the ME coefficient was higher than 3,000 mV/cm Oe under resonant condition. The promising wideband behavior as a function of frequency occurred in the range of 41–110 kHz where the ME coefficient was higher than 260 mV/cm Oe independent of applied H_{DC}. Under low H_{DC} condition, two different ME states were clearly obtained (Fig. 2.17).

2.7 Conclusions

In this section, a generalized theoretical model for low-frequency ME effects in layered composites was discussed. To describe the composite's physical properties, the exact solution of elastostatic and electrostatic equations were obtained. Expressions for the ME susceptibility and ME voltage coefficient were derived as functions of an interface coupling parameter, constituent phase material parameters, and relative volume fractions of phases. Longitudinal, transverse and in-plane cases were all considered properties. For a bilayer that is an asymmetric structure, the influence of flexural deformations of sample on ME output was estimated.

Predictions of the ME effect for various model composite systems were given including CFO–PZT and lanthanum strontium manganite–PZT. It was shown that ME effect in ferrite–PZT systems is maximum for in-plane magnetic and electric fields. The theoretical estimates of ME parameters were compared with experimental data.

The generalized theory allows for modeling of the low-frequency ME effect in bulk composites. To describe these low-frequency composite properties, an effective medium method was used. Calculation of the ME susceptibility, and ME voltage coefficient were performed as functions of volume fractions and component parameters. Composites with connectivity types 3–0 and 0–3 were considered. Larger ME coefficients were found for 3–0 composites with magnetic and/or electric fields applied along the longitudinal direction. For composites of CFO–PZT, values as high as 4 V/cm Oe were predicted for the longitudinal ME voltage coefficient. For the transverse fields orientation, ME effect was found to be in 2–3.5 times smaller than that for longitudinal orientation. Furthermore, clamping was shown to significantly reduce the ME effect.

We presented a theory for the resonance enhancement of ME interactions at frequencies corresponding to EMR. Frequency dependence for ME voltage coefficients are obtained using the simultaneous solution of electrostatic, magnetostatic, and elastodynamic equations. The ME effect at bending mode in a bilayer is shown to be dependent on boundary conditions. A giant ME interaction at the lowest frequency is predicted for a bilayer fixed at one end and is free to vibrate at the other end. The ME voltage coefficients are estimated from known material parameters (piezoelectric coupling, magnetostriction, elastic constants, etc.) of composite components. It is shown that the ME coupling in the EMR region exceeds the low-frequency value by more than an order of magnitude.

References

Bichurin MI, Petrov VM, Srinivasan G (2002a) Modelling of magnetoelectric effect in ferromagnetic/piezoelectric multilayer composites. Ferroelectrics 280:165

Bichurin MI, Petrov VM, Srinivasan G (2002b) Theory of low-frequency magnetoelectric effects in ferromagnetic-ferroelectric layered composites. J Appl Phys 92:7681

Bichurin MI, Petrov VM, Srinivasan G (2003) Theory of low-frequency magnetoelectric coupling in magnetostrictive-piezoelectric bilayers. Phys Rev B 68:054402

Bichurin MI, Petrov VM, Srinivasan G (2009) Low-frequency magnetoelectric effects in ferrite–piezoelectric nanostructures. J Magn Magn Mater 321:846–849

Gheevarughese V, Laletsin U, Petrov VM, Srinivasan G, Fedotov NA (2007) Low-frequency and resonance magnetoelectric effects in lead zirconate titanate and single-crystal nickel zinc ferrite bilayers. J Mater Res 22:2130–2135

Harshe G, Dougherty JO, Newnham RE (1993a) Theoretical modelling of multilayer magnetoelectric composites. Int J Appl Electromagn Mater 4:145

Harshe G, Dougherty JP, Newnham RE (1993b) Theoretical modelling of 3–0, 0–3 magnetoelectric composites. Int J Appl Electromagn Mater 4:161

Mandal SK, Sreenivasulu G, Petrov VM, Srinivasan G (2011) Magnetization-graded multiferroic composite and magnetoelectric effects at zero bias. Phys Rev B 84:014432

Newnham RE, Skinner DP, Cross LE (1978) Connectivity and piezoelectric-pyroelectric composites. Mater Res Bull 13:525

Osaretin IA, Rojas RG (2010) Theoretical model for the magnetoelectric effect in magnetostrictive/piezoelectric composites. Phys Rev B 82:174415

Park C-S, Avirovik D, Bichurin MI, Petrov VM, Priya S (2012) Tunable magnetoelectric response of dimensionally gradient laminate composites. Appl Phys Lett 100:212901

Petrov VM, Srinivasan G (2008) Enhancement of magnetoelectric coupling in functionally graded ferroelectric and ferromagnetic bilayers. Phys Rev B 78:184421

Petrov M, Bichurin MI, Laletin VM, Paddubnaya N, Srinivasan G (2004) Modeling of magnetoelectric effects in ferromagnetic/piezoelectric bulk composites. In: Fiebig M, Eremenko VV, Chupis IE (eds) Magnetoelectric interaction phenomena in crystals-NATO science series II, vol 164. Kluwer Academic Publishers, London, pp 65–70

Petrov VM, Srinivasan G, Laletsin U, Bichurin MI, Tuskov DS (2007) Magnetoelectric effects in porous ferromagnetic-piezoelectric bulk composites: experiment and theory. Phys Rev B 75:174422

Petrov VM, Srinivasan G, Bichurin MI, Galkina TA (2009) Theory of magnetoelectric effect for bending modes in magnetostrictive-piezoelectric bilayers. J Appl Phys 105:063911

http://www.springer.com/978-94-017-9155-7

Modeling of Magnetoelectric Effects in Composites

Bichurin, M.; Petrov, V.

2014, X, 108 p. 60 illus., Hardcover
ISBN: 978-94-017-9155-7